

***Ab initio* electronic stopping power of protons in bulk materials**

Abdullah Atef Shukri and Fabien Bruneval

CEA, DEN, Service de Recherches de Métallurgie Physique, Université Paris-Saclay, F-91191 Gif-sur-Yvette, France

Lucia Reining

Laboratoire des Solides Irradiés, École Polytechnique, CNRS, CEA-DSM-IRAMIS, Université Paris-Saclay, F-91128 Palaiseau, France and European Theoretical Spectroscopy Facility (ETSF)

(Received 3 November 2015; revised manuscript received 5 January 2016; published 21 January 2016)

The electronic stopping power is a crucial quantity for ion irradiation: it governs the deposited heat, the damage profile, and the implantation depth. Whereas experimental data are readily available for elemental solids, the data are much more scarce for compounds. Here we develop a fully *ab initio* computational scheme based on linear response time-dependent density-functional theory to predict the random electronic stopping power (RESP) of materials without any empirical fitting. We show that the calculated RESP compares well with experimental data, when at full convergence, with the inclusion of the core states and of the exchange correlation. We evaluate the unexpectedly limited magnitude of the nonlinear terms in the RESP by comparing with other approaches based on the time propagation of time-dependent density-functional theory. Finally, we check the validity of a few empirical rules of thumbs that are commonly used to estimate the electronic stopping power.

DOI: [10.1103/PhysRevB.93.035128](https://doi.org/10.1103/PhysRevB.93.035128)**I. INTRODUCTION**

The stopping power of an irradiating ion in condensed matter is defined as the kinetic energy loss per unit of path length:

$$S = -\frac{dE}{dx}. \quad (1)$$

This quantity is central to many technological fields that involve particle irradiation. Besides for materials in nuclear or space environments [1] the stopping power is highly relevant for the depth of implantation of dopants in electronics [2] and for the accurate prediction of damage in the proton therapy used in nuclear medicine [3]. Due to its importance, the stopping power of ions has been the subject of intense research for the last 80 years [4].

The stopping power consists of two components: the nuclear stopping power S_n , which involves energy losses due to collisions with the nuclei of the target, and the electronic stopping power S_e , which arises from the excitation of the electrons of the target. As soon as the kinetic energy of the impinging ion is larger than a few tens of keV/amu, the electronic part becomes the vastly dominating contribution [5].

Historically, the electronic stopping power has been first evaluated with model scattering formulas [6–8]. This was followed by the calculations based on the free-electron gas (FEG), pioneered by Lindhard [9]. The electron gas modeling and its further refinements have been continuously used since then [10–14]. More recently, with the advent of density-functional theory and its time-dependent version (TDDFT) [15], the fully *ab initio* evaluation of the random electronic stopping power (RESP) has become within reach [16–22].

Among the recent applications of TDDFT to the calculation of stopping power, two frameworks have emerged: one is in the linear response regime, in which the response functions are expressed in terms of the frequency; the second is based on the time-propagation approach, in which the time-dependent

Kohn-Sham (KS) equations have to be solved [23]. Both approaches have advantages and limitations. Time propagation incorporates the response to all orders and this is expected to yield important contributions at low velocity. However, the time discretization needs to be monitored [24–26] and supercells have to be employed. This leads to very cumbersome calculations. The linear-response framework is simpler, though it still requires careful monitoring of the convergence. Moreover, the limitation to the linear terms might be questionable for the low ion velocities and for projectiles with a higher charge. The need for nonlinear terms to correctly capture the dependence on the charge of the projectile has been known for decades [27,28]. A striking illustration of the limitation of the linear-response approximation is its failure to describe the proton/antiproton asymmetry [19,20]. However, a complete exploration of the linear-response theory for realistic materials is still missing today.

In this work, we propose to push the linear-response approach to its limit and appreciate its range of validity to evaluate the RESP. We aim at exploring the power of the calculations to predict experimental results, since the experimental data are scarce for nonelemental crystals. Due to the slow convergence of the calculations in practice, we are careful about producing fully converged *ab initio* electronic stopping power within linear-response theory. The agreement with time-propagation results is surprisingly good as we will show. We furthermore evaluate the validity of a few empirical rules of thumb that are often used in practice, such as the Bragg's additivity rule or the bond effect.

The article is organized as follows: Sec. II is a general presentation of the linear response TDDFT formalism applied to the RESP. Sec. III details the practical implementation in plane waves and proposes a working approach to achieve convergence. Section IV presents the effect of the physical approximations on the RESP. Section V discusses the validity of a few empirical rules. Conclusions are given in Sec. VI. Hartree atomic units will be used throughout the text ($\hbar = e = a_0 = 1$).

II. LINEAR RESPONSE FORMALISM FOR THE STOPPING POWER

In this section, we quickly recap the main computational steps that allow one to evaluate the random electronic stopping power in a periodic plane-wave formalism within linear response theory.

A. Linear response TDDFT

In a landmark paper, Petersilka *et al.* [15] derived the TDDFT equations within the linear response theory. Solving TDDFT in linear response is tantamount to solving a Dyson-like equation that relates the noninteracting Kohn-Sham polarizability χ^{KS} to the fully interacting polarizability χ . In a periodic material, this equation can be cast into a matrix form when expressed in plane waves:

$$\chi_{\mathbf{G}\mathbf{G}'}(\mathbf{q},\omega) = \chi_{\mathbf{G}\mathbf{G}'}^{\text{KS}}(\mathbf{q},\omega) + \sum_{\mathbf{G}_1, \mathbf{G}_2} \chi_{\mathbf{G}\mathbf{G}_1}^{\text{KS}}(\mathbf{q},\omega) \times f_{H_{xc}\mathbf{G}_1, \mathbf{G}_2}(\mathbf{q},\omega) \chi_{\mathbf{G}_2\mathbf{G}'}(\mathbf{q},\omega), \quad (2)$$

where \mathbf{G} are reciprocal lattice vectors and \mathbf{q} is a vector in the first Brillouin zone (BZ). It should be understood that the notation $\chi_{\mathbf{G}\mathbf{G}'}(\mathbf{q},\omega)$ is shorthand for $\chi_{\mathbf{G}\mathbf{G}'}(\mathbf{q} + \mathbf{G}, \mathbf{q} + \mathbf{G}', \omega)$. The kernel of the equation $f_{H_{xc}}$ consists of a Hartree part

$$v(\mathbf{q} + \mathbf{G}) = \frac{4\pi}{|\mathbf{q} + \mathbf{G}|^2} \quad (3)$$

and of the so-called exchange-correlation kernel f_{xc} , which is the functional derivative of the Kohn-Sham exchange-correlation potential with respect to the density. In the present work, we will use only very simple approximations to f_{xc} : either the random-phase approximation that completely neglects f_{xc} or the adiabatic local-density approximation (ALDA) that assumes a local dependence on the density, in space and in time.

The Kohn-Sham polarizability is obtained through the Adler-Wiser formula [29,30]:

$$\chi_{\mathbf{G}\mathbf{G}'}^{\text{KS}}(\mathbf{q},\omega) = \frac{2}{N_{\mathbf{k}}\Omega} \sum_{\substack{\mathbf{k} \\ i,j}} (f_{\mathbf{k}-\mathbf{q}i} - f_{\mathbf{k}j}) \times \frac{M_{\mathbf{k}ij}(\mathbf{q} + \mathbf{G})M_{\mathbf{k}ij}^*(\mathbf{q} + \mathbf{G}')}{\omega - (\epsilon_{\mathbf{k}j} - \epsilon_{\mathbf{k}-\mathbf{q}i}) + i\eta}, \quad (4)$$

where the matrix elements read

$$M_{\mathbf{k}ij}(\mathbf{q} + \mathbf{G}) = \langle \mathbf{k} - \mathbf{q}i | e^{-i(\mathbf{q}+\mathbf{G})\cdot\mathbf{r}} | \mathbf{k}j \rangle. \quad (5)$$

Here, Ω stands for the unit cell volume, and $N_{\mathbf{k}}$ for the number of \mathbf{k} points in the BZ. $f_{\mathbf{k}i}$ and $\epsilon_{\mathbf{k}i}$ are, respectively, the occupations and the energies of the KS state $|\mathbf{k}i\rangle$ with band index i and wave vector \mathbf{k} .

The inverse dielectric matrix is defined as the functional derivative of the total Kohn-Sham potential $v_{\text{KS}}(\mathbf{r},t)$ with respect to the external potential $v_{\text{ext}}(\mathbf{r}',t')$. In reciprocal space, it can be linked to the polarizability χ with a matrix

equation:

$$\epsilon_{\mathbf{G}\mathbf{G}'}^{-1}(\mathbf{q},\omega) = \delta_{\mathbf{G}\mathbf{G}'} + v(\mathbf{q} + \mathbf{G})\chi_{\mathbf{G}\mathbf{G}'}(\mathbf{q},\omega). \quad (6)$$

The imaginary part of the inverse dielectric matrix is central to describe the loss processes involved in electron energy loss spectroscopy [31] or in inelastic x-ray scattering [32,33].

B. Dielectric matrix expression of the random electronic stopping power

Since the inverse frequency-dependent dielectric matrix contains the loss function, it is also the central quantity to quantify the slowing down of a charged particle in a condensed matter target within linear response. As the matter is quite delicate, we would like to seize the opportunity to reproduce a full derivation of the random electronic stopping power in the exact form it can be implemented in a plane-wave formalism. A similar derivation can be found in Ref. [34] for instance.

Describing an impinging particle with electric charge Z_1 as a classical point charge moving at constant velocity \mathbf{v} with impact parameter \mathbf{b} , its density reads

$$\rho_{\text{ext}}(\mathbf{r},t) = Z_1 \delta(\mathbf{r} - \mathbf{b} - \mathbf{v}t). \quad (7)$$

The power dissipated in a medium is measured by the classical formula:

$$\frac{dE}{dt} = \int d\mathbf{r} \mathbf{j}_{\text{ext}}(\mathbf{r},t) \cdot \mathbf{E}(\mathbf{r},t), \quad (8)$$

where \mathbf{E} is the total electric field and \mathbf{j}_{ext} is the charge current of the impinging particle. As we consider a point charge with constant velocity \mathbf{v} , the charge current can simply be written $\mathbf{j}_{\text{ext}}(\mathbf{r},t) = \rho_{\text{ext}}(\mathbf{r},t)\mathbf{v}$. If the x axis is taken along the velocity, $x = vt$ and we can apply the chain rule to link Eq. (8) to the definition of the stopping power in Eq. (1):

$$S_e(\mathbf{v},\mathbf{b}) = -\frac{1}{v} \int d\mathbf{r} \rho_{\text{ext}}(\mathbf{r},t)\mathbf{v} \cdot \mathbf{E}(\mathbf{r},t), \quad (9)$$

where we have highlighted the dependence on the impact parameter \mathbf{b} . $S_e(\mathbf{v},\mathbf{b})$ is called the position-dependent stopping power.

Let us express the total electric field as a function of the external density. The electric field derives from a potential $\phi_{\text{tot}}(\mathbf{r},t)$ following

$$\mathbf{E}(\mathbf{r},t) = -\nabla_{\mathbf{r}}\phi_{\text{tot}}(\mathbf{r},t). \quad (10)$$

Note that the electric potential used here differs by a sign from the electronic potentials v_{KS} and v_{ext} introduced in Sec. II A.

Equation (10) can be conveniently written in the Fourier space:

$$\mathbf{E}(\mathbf{r},t) = -\frac{1}{2\pi N_{\mathbf{k}}\Omega} \sum_{\mathbf{q}} \sum_{\mathbf{G}} i(\mathbf{q} + \mathbf{G}) \times \int d\omega e^{i(\mathbf{q}+\mathbf{G})\cdot\mathbf{r} - i\omega t} \phi_{\text{tot}}(\mathbf{q} + \mathbf{G},\omega), \quad (11)$$

where the Fourier transform of the electric potential $\phi_{\text{tot}}(\mathbf{q} + \mathbf{G},\omega)$ has been introduced.

The ratio between the electric potential ϕ_{tot} and the external potential ϕ_{ext} is measured by the inverse dielectric matrix that has been introduced earlier in Sec. II A. Thus, the electric potential can be expressed as

$$\phi_{\text{tot}}(\mathbf{q} + \mathbf{G}, \omega) = \sum_{\mathbf{G}'} \varepsilon_{\mathbf{G}\mathbf{G}'}^{-1}(\mathbf{q}, \omega) \phi_{\text{ext}}(\mathbf{q} + \mathbf{G}', \omega), \quad (12)$$

and the external potential, in turn, can be calculated from the Poisson equation:

$$\phi_{\text{ext}}(\mathbf{q} + \mathbf{G}', \omega) = \frac{4\pi}{|\mathbf{q} + \mathbf{G}'|^2} 2\pi Z_1 \times \delta[\omega - \mathbf{v} \cdot (\mathbf{q} + \mathbf{G}')] e^{-i\mathbf{b} \cdot (\mathbf{q} + \mathbf{G}')}. \quad (13)$$

The Fourier transform of the point charge $\rho_{\text{ext}}(\mathbf{r}, t)$ has been introduced. With this, we have indeed written the electric field $\mathbf{E}(\mathbf{r}, t)$ in terms of the external density.

Gathering the results from Eqs. (11)–(13), the integrations over \mathbf{r} and ω in Eq. (9) can be performed analytically to yield

$$S_e(\mathbf{v}, \mathbf{b}) = \frac{i4\pi Z_1^2}{N_{\mathbf{k}} \Omega v} \sum_{\mathbf{q}} \sum_{\mathbf{G}\mathbf{G}'} \varepsilon_{\mathbf{G}\mathbf{G}'}^{-1}[\mathbf{q}, \mathbf{v} \cdot (\mathbf{q} + \mathbf{G}')] \times \frac{\mathbf{v} \cdot (\mathbf{q} + \mathbf{G})}{|\mathbf{q} + \mathbf{G}'|^2} e^{-i(\mathbf{G}' - \mathbf{G}) \cdot \mathbf{b}} e^{-i(\mathbf{G}' - \mathbf{G}) \cdot \mathbf{v}\mathbf{t}}. \quad (14)$$

The last exponential in the previous equation is an oscillatory term that gives no contribution if averaged over a long period of time, except for those vectors $(\mathbf{G}' - \mathbf{G})$ that are perpendicular to the velocity \mathbf{v} . Let us label \mathbf{J}_{\perp} such a vector. Hence, Eq. (14) can be recast into

$$S_e(\mathbf{v}, \mathbf{b}) = \frac{i4\pi Z_1^2}{N_{\mathbf{k}} \Omega v} \sum_{\mathbf{q}} \sum_{\mathbf{G}\mathbf{J}_{\perp}} \varepsilon_{\mathbf{G}\mathbf{G} + \mathbf{J}_{\perp}}^{-1}[\mathbf{q}, \mathbf{v} \cdot (\mathbf{q} + \mathbf{G} + \mathbf{J}_{\perp})] \times \frac{\mathbf{v} \cdot (\mathbf{q} + \mathbf{G})}{|\mathbf{q} + \mathbf{G} + \mathbf{J}_{\perp}|^2} e^{-i\mathbf{J}_{\perp} \cdot \mathbf{b}}. \quad (15)$$

This is the final expression for the position-dependent electronic stopping power. This expression can describe for instance the channeling effect of an ion traveling through the voids of a crystalline structure.

Then the random electronic stopping power, the quantity we are interested in this paper, is derived from the position-dependent electronic stopping power by averaging over the impact parameter. The oscillatory term in Eq. (15) is nonvanishing only when $\mathbf{J}_{\perp} = 0$. This observation yields the final result:

$$S_e(\mathbf{v}) = \frac{i4\pi Z_1^2}{N_{\mathbf{k}} \Omega v} \sum_{\mathbf{q}} \sum_{\mathbf{G}} \varepsilon_{\mathbf{G}\mathbf{G}}^{-1}[\mathbf{q}, \mathbf{v} \cdot (\mathbf{q} + \mathbf{G})] \times \frac{\mathbf{v} \cdot (\mathbf{q} + \mathbf{G})}{|\mathbf{q} + \mathbf{G}|^2}. \quad (16)$$

This last result can be further refactored in order to highlight that the stopping power is indeed real valued. Using the fact that the response function $\varepsilon^{-1}(\mathbf{r}\mathbf{t}, \mathbf{r}'\mathbf{t}')$ is real valued, its Fourier transform has the following symmetry (see Appendix A of Ref. [34] for a derivation):

$$\varepsilon_{\mathbf{G}\mathbf{G}'}^{-1}(\mathbf{q}, \omega) = [\varepsilon_{-\mathbf{G}-\mathbf{G}'}^{-1}(-\mathbf{q}, -\omega)]^*. \quad (17)$$

Then, for each $\mathbf{q} + \mathbf{G}$ that appears in the summation in Eq. (16), the corresponding $-\mathbf{q} - \mathbf{G}$ will be part of the summation as

well. As a consequence, only the imaginary part of ε^{-1} yields a contribution to the summation and the RESP can be finally recast into

$$S_e(\mathbf{v}) = \frac{4\pi Z_1^2}{N_{\mathbf{k}} \Omega v} \sum_{\mathbf{q}} \sum_{\mathbf{G}} \text{Im}\{-\varepsilon_{\mathbf{G}\mathbf{G}}^{-1}[\mathbf{q}, \mathbf{v} \cdot (\mathbf{q} + \mathbf{G})]\} \times \frac{\mathbf{v} \cdot (\mathbf{q} + \mathbf{G})}{|\mathbf{q} + \mathbf{G}|^2}. \quad (18)$$

This expression for S_e is identical to the formula published by Campillo *et al.* [16] [see their Eq. (3.11)], apart from an overall factor 2. Our Eq. (18) correctly reduces to the Lindhard formula for the specific case of a homogeneous system as shown in the Appendix. However, our numerical results do agree with Campillo and co-workers as we will show in the next section.

III. PRACTICAL IMPLEMENTATION IN A PERIODIC PLANE-WAVE APPROACH

Many modern *ab initio* codes for periodic systems are capable of calculating the inverse dielectric matrix $\varepsilon_{\mathbf{G}\mathbf{G}'}^{-1}(\mathbf{q}, \omega)$ for finite frequencies ω . For instance, this quantity is requested in the *GW* framework [35,36]. The present work relies on the *GW* subroutine available in the ABINIT software [37].

A. Technicalities

As we will show in the following, the convergence of the stopping power with respect to the parameters of the calculation is strikingly slow even for systems with a small unit cell. This makes the use of symmetry operations absolutely crucial to perform calculations on an affordable time scale.

Equation (18) can be rewritten with the use of the symmetries \mathcal{R} contained in the crystal space group that produce the star of \mathbf{q} vectors. With this, Eq. (18) reads

$$S_e(\mathbf{v}) = \frac{4\pi Z_1^2}{N_{\mathbf{k}} \Omega v} \sum_{\mathbf{q}} \sum_{\mathcal{R} \in \mathcal{R}_{\mathbf{q}}} \text{Im}\{-\varepsilon_{\mathcal{R}\mathbf{G}, \mathcal{R}\mathbf{G}}^{-1}[\mathbf{q}, \mathbf{v} \cdot (\mathcal{R}\mathbf{q} + \mathbf{G})]\} \times \frac{\mathbf{v} \cdot (\mathcal{R}\mathbf{q} + \mathbf{G})}{|\mathcal{R}\mathbf{q} + \mathbf{G}|^2}, \quad (19)$$

where the summation over \mathbf{q} only runs over the irreducible wedge of the Brillouin zone (IBZ).

Furthermore, the inverse dielectric matrix needs to be evaluated for many energies $\omega = \mathbf{v} \cdot \mathbf{q} + \mathbf{G}$. It would be almost intractable to calculate and invert the dielectric matrix for each requested ω . We rather calculate and invert the dielectric matrix on a dense grid of frequencies and then perform a cubic spline interpolation in order to evaluate its diagonal at the desired energy.

Because of the discrete sampling of the BZ, the imaginary part of the inverse dielectric matrix is a rather noisy function of the energy, which can be smoothed with an increase of the broadening η in Eq. (4). Due to the spline interpolation,

the number of sampling energies becomes a parameter to be converged.

B. Assessment against previous calculations

In order to assess our calculation method, we first checked our results against the only series of articles [16–18] we are aware of that implemented the linear-response RESP from fully *ab initio* calculations in periodic systems. Using our norm-conserving pseudopotential implementation in ABINIT, we calculated the RESP of bulk silicon and bulk aluminum at their experimental lattice constant.

Carefully following the technical details of Ref. [18], we used the same convergence parameters in order to offer a direct comparison in Fig. 1. As the authors of Ref. [18] point out themselves, these results are not converged well enough to permit comparison with experiment. In Fig. 1, we just aim at demonstrating the correctness of the implementation.

Silicon and aluminum are described by valence electron only norm-conserving pseudopotentials. The dielectric matrices have been limited to a 15×15 representation in plane waves, corresponding to an energy cutoff of 0.75 Ha in silicon and of 1.35 Ha in aluminum. The number of bands is limited to 200 for silicon and to 60 in aluminum. The \mathbf{k} -point mesh is $8 \times 8 \times 8$ for Si and $10 \times 10 \times 10$ for Al. Finally, whereas Ref. [18] employs an analytic continuation technique that extrapolates the inverse dielectric function from purely imaginary frequencies to purely real frequencies, our work relies on a direct evaluation of the response functions for real frequencies. However, we have to employ a finite value for the broadening parameter η entering in Eq. (4). A value $\eta = 1.5$ eV was used to produce the the data reported in Fig. 1.

Despite the difference in the sampling of the inverse dielectric matrix, the agreement between our calculations and the previously published results is very good, which also indicates that the data published in Ref. [18] are consistent with our Eq. (18).

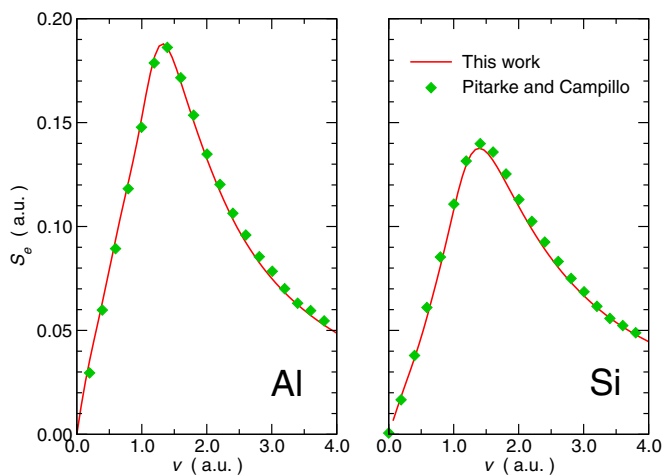


FIG. 1. Comparison of the RESP of a proton within RPA from our implementation (solid red line) against previously published results from Ref. [18] (green diamonds). The calculations are converged with the same level of accuracy as prescribed in the previous work.

C. Convergence issues

As already alluded to in the previous paragraph, the calculation of RESP requires extremely large convergence parameters that were not accessible 15 years ago and that are still challenging nowadays.

First, we set the convergence with respect to the frequency sampling grid, which can be easily handled. The maximum frequency for $\chi^{\text{KS}}(\omega)$ is determined by the maximum velocity \mathbf{v} and the dielectric matrix cutoff E_{cut} through $\omega_{\text{max}} \approx |\mathbf{G}_{\text{max}}| \times |\mathbf{v}_{\text{max}}|$. Then the frequency grid sampling is found to be very well converged with six points per Hartree for all the systems we study here.

In Fig. 2, we show the convergence of the RESP as a function of the other parameters. The parameters can be grouped into two independent sets: the number of bands N_b and the dielectric matrix cutoff E_{cut} on one side (left-hand panel of Fig. 2) and the \mathbf{k} -point and \mathbf{q} -point sampling on the other side (right-hand panel of Fig. 2).

First of all, as a general comment, the convergence of RESP appears as extremely slow compared to the convergence parameters required in ground-state DFT or even in standard excited state calculations within TDDFT. The number of bands necessary to converge the RESP up to velocity $v = 4$ a.u. (which corresponds to a proton at 0.4 MeV) is around 1500, to be compared to the four occupied bands of silicon. The converged dielectric matrix cutoff energy is 25 Ha, to be compared to the cutoff energy for wave functions in norm-conserving pseudopotential of about 10 Ha. The RESP peak necessitates at least 864 \mathbf{k} points in the BZ, which corresponds to a $6 \times 6 \times 6$ Monkhorst-Pack grid with four different origins, whereas standard calculations usually require only 256 \mathbf{k} points in the BZ ($4 \times 4 \times 4$ grid with four shifts).

The extremely slow convergence with respect to these parameters has two different origins that can be ascribed to

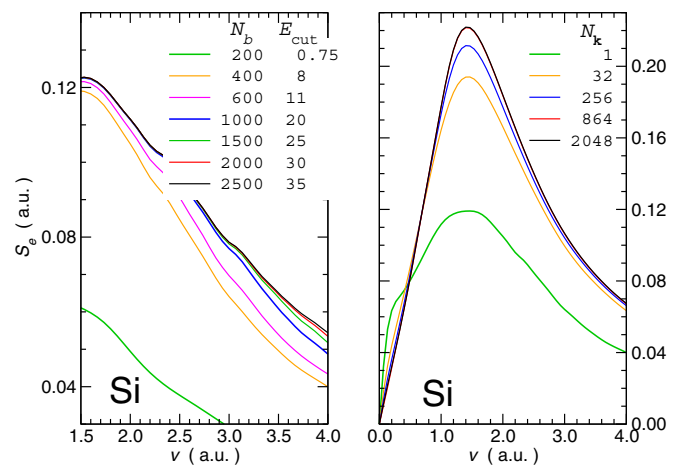


FIG. 2. Convergence of the RESP of a proton in silicon within RPA as a function of the number of bands and of the dielectric matrix cutoff in the left-hand panel and as a function of \mathbf{k} points in the right-hand panel. The convergence with respect to N_b and E_{cut} was obtained with a fixed Γ -point sampling, whereas the convergence with respect to the \mathbf{k} -point grid was evaluated for a fixed number of bands (400) and a fixed dielectric matrix cutoff (8 Ha).

the different equations presented in Sec. II. That is why we grouped the convergence parameters into two sets.

First, the dielectric matrix cutoff and the number of bands are tightly related as can be inferred from the matrix element in Eq. (5). If high-energy empty bands are included in the sum of states formula of χ^{KS} , the representation of these states in plane wave involves high-energy plane waves. These high plane waves are coupled with the occupied states through large reciprocal lattice vectors \mathbf{G} in Eq. (5). This observation justifies why the convergence with respect to bands and to the dielectric matrix cutoff cannot be evaluated independently. In Fig. 2, we have shown the RESP curves for the converged dielectric matrix cutoff associated with a given number of bands. For instance, for 400 bands, a dielectric matrix cutoff of 8 Ha is sufficient. However, for 1500 bands, it should rather be set to 25 Ha.

Secondly, the BZ sampling appears through the \mathbf{k} points in Eq. (4) and through the \mathbf{q} points in Eq. (18). Whereas the \mathbf{q} points are only constrained to be differences of \mathbf{k} points due to the evaluation of the matrix elements in Eq. (5), we have limited ourselves to the very same grids for both \mathbf{k} and \mathbf{q} points since a down-sampling analogous to Ref. [38] would have induced marginal computational gains only. The convergence with respect to \mathbf{k} points in Eq. (4) is made smoother thanks to a well adapted value of the broadening parameter η . For instance, in the right-hand panel of Fig. 2, the curve with Γ point was obtained $\eta = 12$ eV, while the result with 2048 points used $\eta = 1$ eV.

D. Extrapolation scheme

As the convergence is difficult to obtain and as the convergence factors have different origins, it is legitimate to evaluate the possibility to reach the global convergence by adding up the different contributions. To this aim we extrapolate the RESP using the formula

$$S_e(\text{extrap.}) = S_e(N_b, E_{\text{cut}} = \text{low}, N_k = \text{high}) + S_e(N_b, E_{\text{cut}} = \text{high}, N_k = \text{low}) - S_e(N_b, E_{\text{cut}} = \text{low}, N_k = \text{low}), \quad (20)$$

where low/high characterizes the convergence level for the number of bands N_b and dielectric matrix cutoff E_{cut} on one side and for the \mathbf{k} -point grid on the other side.

In Fig. 3, we demonstrate that the extrapolation is indeed justified. Calculations obtained for two levels of convergence are shown in the upper panel of Fig. 3 for two different \mathbf{k} -point meshes. The better converged calculation uses $N_b = 600$ and $E_{\text{cut}} = 11$ Ha, while the less converged calculations have $N_b = 400$ and $E_{\text{cut}} = 8$ Ha. In the lower panel, we evaluated the difference between these two levels of convergence, either with a Γ -point sampling (red line) or with a much denser sampling (864 \mathbf{k} points). The small difference of the curves for the two \mathbf{k} -point samplings in the lower panel of Fig. 3 demonstrates that a coarse \mathbf{k} -point sampling is indeed sufficient to capture the slow convergence with respect to N_b and E_{cut} as proposed in Eq. (20).

With these techniques at hand, we are now ready to calculate RESP that are converged in absolute.

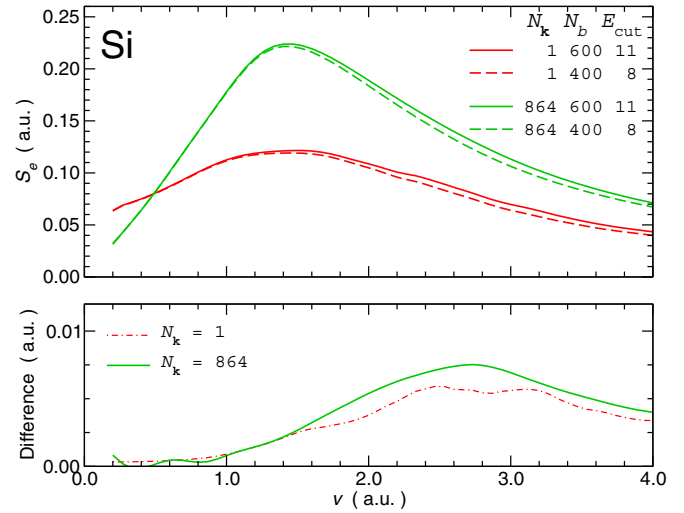


FIG. 3. Comparison of the convergence rate of the RESP of a proton in silicon for two \mathbf{k} -point meshes: Γ (red lines) and 864 BZ points (green lines). The upper panel shows the RESP for two levels of convergence. The lower panel shows the difference between the curve that is better converged with respect to N_b and N_k minus the curve that is less converged for the two \mathbf{k} -point meshes.

IV. PHYSICAL APPROXIMATIONS RELEVANT FOR BULK MATERIALS

A. Ab initio against models based on the free-electron gas

Random-phase approximation (RPA) calculations in real materials are still very challenging. We have just seen that the convergence issues are dramatic. Therefore, models based on the FEG have been developed and used with relative success in the previous 50 years [9,10,12–14].

We propose to examine here the validity of these models against the calculated *ab initio* RPA for silicon, as shown in Fig. 4. The crudest modeling we consider is the analytic

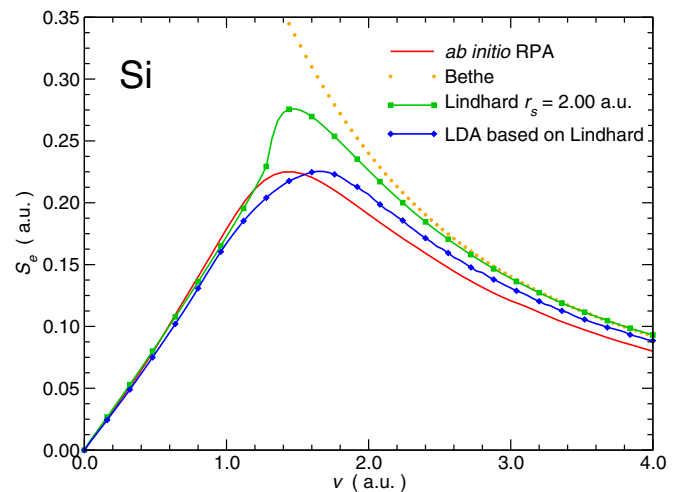


FIG. 4. FEG-based modeling of the RESP of a proton in silicon against the reference *ab initio* RPA calculation.

formula of Bethe [7]:

$$S_e^{\text{Bethe}}(v) = \frac{Z_1^2 \omega_p^2}{v^2} \ln\left(\frac{2v^2}{\omega_p}\right), \quad (21)$$

where $\omega_p = \sqrt{4\pi\rho_0}$ is the classical plasma frequency and ρ_0 is the average electronic density. In Fig. 4, the Bethe formula is not evaluated for $v < 1$ a.u., since the formula shows a divergence there. However, the Bethe formula properly captures the large v behavior. The Bethe formula can be tuned with a mean ionization energy I inserted in the denominator in the logarithm [39–41], but still the description is still not adequate at the low velocities.

A huge improvement is due to Lindhard [9], who derived the RPA RESP formula for a FEG at a given homogeneous electron density ρ_0 . The Lindhard RESP still requires a numerical evaluation of a double integral [10]. Figure 4 shows the Lindhard RESP evaluated at the same average density as the valence electrons of bulk silicon ($r_s = 2.00$ a.u.). The Lindhard RESP deviates noticeably from the *ab initio* RPA, especially around the peak at $v = 1.4$ a.u. However, contrary to the Bethe formula, the overall slope is now correct.

A route to improve the description of real inhomogeneous solids is the local-density approximation (LDA) to RESP [10,42]. This approximation assumes that the RESP of a solid can be obtained as the spatial average over the Lindhard RESP evaluated at the local density $\rho(\mathbf{r})$:

$$S_e(v) \approx \frac{1}{\Omega} \int_{\Omega} d\mathbf{r} S_e^{\text{Lindhard}}(\rho(\mathbf{r}), v). \quad (22)$$

Using the valence density as obtained from the *ab initio* calculation, Fig. 4 shows that the LDA based on Lindhard produces a rather meaningful evaluation of the RESP of Si. However, as we will see next, LDA based on Lindhard is not adequate when including the tightly bound core electrons.

B. RPA versus ALDA

Even the *ab initio* RPA results do not compare well with experiment yet. As exemplified in Fig. 5 for silicon, the RPA evaluation of RESP largely underestimates the experimental reference results.

We have so far employed the simplest approximation to the TDDFT kernel, that it is its complete neglect. Whereas other simple TDDFT kernels, such as ALDA, are known to have very little effect on the optical spectra in solids [31,44,45], it has been shown in previous works that ALDA brings a significant improvement for the dynamic structure factor $S(\mathbf{Q}, \omega)$ as compared to inelastic x-ray scattering [32,33]. The structure factor is proportional to an individual element of the inverse dielectric matrix diagonal and the stopping power S_e is an integral over these elements. A good description of the dynamic structure factor should then lead to success in predicting the RESP.

Figure 5 demonstrates how the inclusion of the ALDA kernel significantly increases the RESP in the low velocity regime. However, for the larger velocities $v > 2$ a.u., the RESP is completely insensitive to the TDDFT kernel. In other words, thanks to ALDA, the agreement with respect to experiment is excellent for low velocities up to the maximum of the peak,

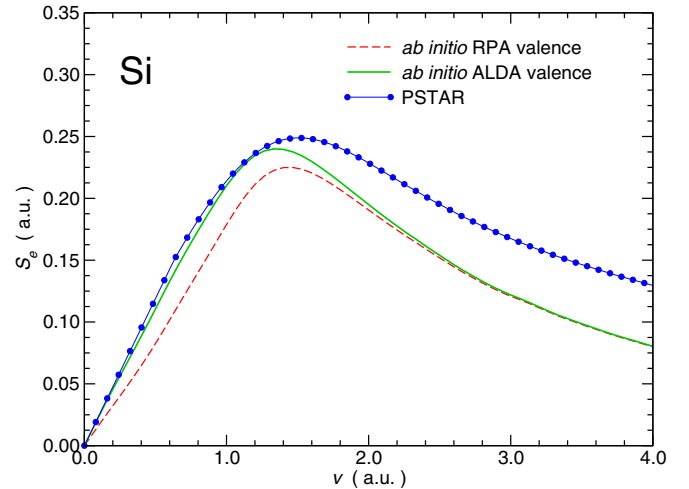


FIG. 5. RESP of a proton in silicon using different approximations for the TDDFT kernel: RPA (dashed red line) and ALDA (solid green line). Silicon is described by its valence electrons only. Experiment from the PSTAR database [43] (blue circles) is given as a reference.

but the stopping power still remains largely underestimated for higher velocities.

C. Contribution of the core states

To address the underestimation of the RESP for large velocities, the natural step is to include the description of the core states. Indeed, we have shown in Sec. III that the RESP is very sensitive to the high-energy transitions included in the response χ^{KS} and that a huge number of empty bands is necessary to achieve convergence. In an analogous manner, the RESP can be expected to be much affected by core electrons. For instance, in silicon, the $2s$ and $2p$ electrons are located about 100 eV below the valence and can contribute to the loss processes for moderate values of the velocity v . The $1s$ electrons which lie 1700 eV below the valence can instead be disregarded.

The effect of the $2s2p$ electrons of Si on the RESP can be appreciated from Fig. 6, where the calculations with two pseudopotentials with or without $2s$ and $2p$ in the valence have been carried out. The $2s2p$ electrons yield a significant additional contribution to the RESP for velocities beyond 1.5 a.u., whereas they have no effect below. However, even when introducing the core electrons, the RESP for high velocity is underestimated by about 10%–15% with respect to experiment.

Unfortunately, the calculations with explicit core states not only have more occupied states in the summation of Eq. (4), but also have a much harder pseudopotential, that in turn induces a higher dielectric matrix cutoff. Silicon now requires $E_{\text{cut}} = 35$ Ha instead of 25 Ha. With such a high computational burden, it would be desirable to have an approximate scheme to handle the core states.

Let us analyze further here the contribution from the core electrons alone. In the lower panel of Fig. 7, we evaluate the contribution of the core electrons to the RESP of Si for different approximations as the difference between the RESP curves

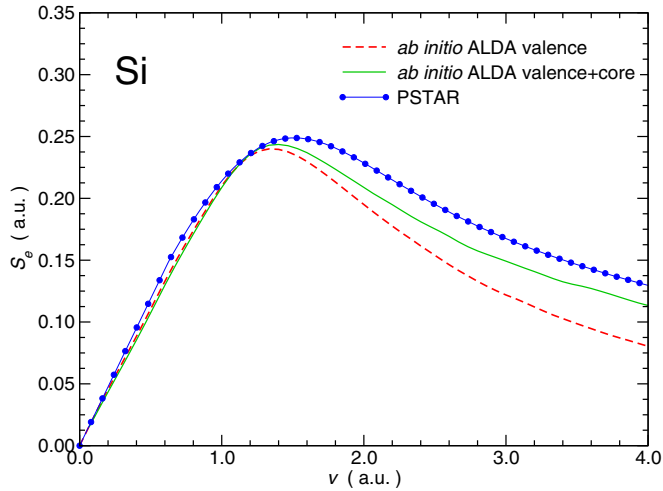


FIG. 6. RESP of a proton in silicon within ALDA including (solid green line) or not (dashed red line) the contribution from the core $2s$ and $2p$ electrons. Experiment from the PSTAR database [43] (blue circle symbols) is given as a reference.

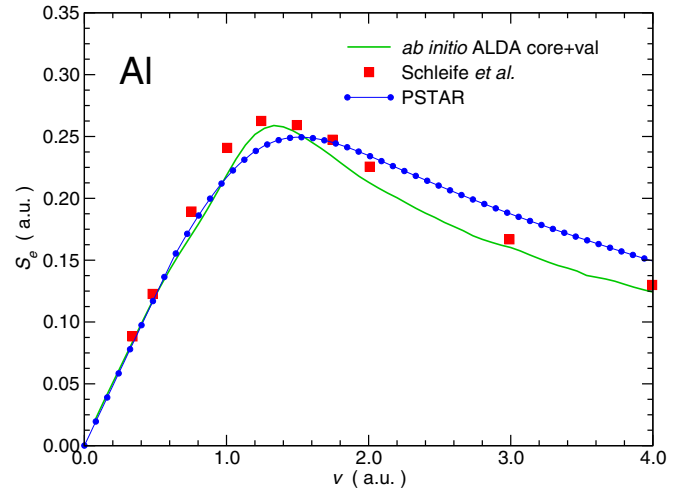


FIG. 8. RESP of a proton in Al within ALDA in linear response (solid green line) compared to the time-propagation results of Schleife and co-authors [22]. Experiment from the PSTAR database [43] (blue circle symbols) is given as a reference.

obtained in the upper panel. In contrast with the statement issued for valence electrons, the effect of the ALDA kernel is negligible. The ALDA and the RPA core RESP differ by at most 0.005 a.u. which is to be compared with the value of the total RESP of 0.1–0.2 a.u. for the depicted range of velocities.

We also considered the opportunity to have a cheap evaluation of the core contribution using the LDA based on the Lindhard stopping power. In the upper panel of Fig. 7, the LDA RESP is calculated for both the valence electronic density and the valence plus core electronic density. The difference between the two can be compared with the full *ab initio* calculation in the lower panel. The LDA technique is not

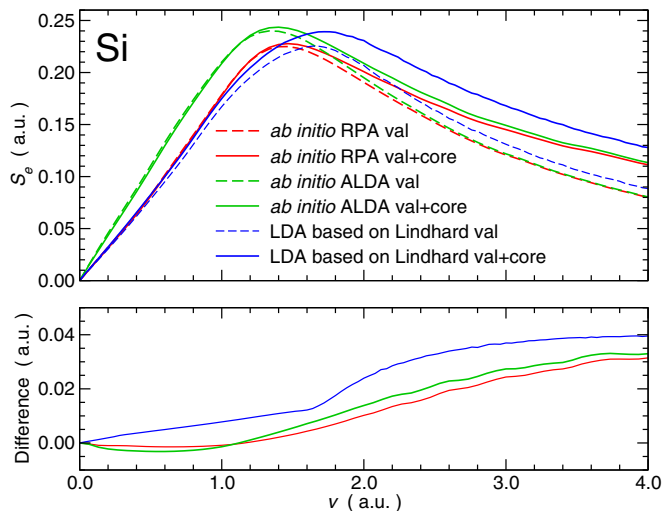


FIG. 7. Upper panel: RESP of a proton in silicon within RPA (red lines), ALDA (green lines), and LDA based on Lindhard (blue lines) including (solid lines) or not (dashed lines) the contribution from the core $2s$ and $2p$ electrons. Lower panel: Core-only contribution to the RESP of Si as obtained through the difference between the calculations with and without $2s$ and $2p$ within RPA, ALDA, or LDA based on Lindhard.

perfectly adequate to describe the core contribution. Indeed, the stopping power continuously increases starting from the lowest velocities. In other words, the LDA core misses the shell effect: the core contribution should be zero up to the minimum velocity that allows the core electrons to be excited.

Even though the LDA technique could describe the core contribution with reasonable accuracy, we rather use an explicit introduction of the core electrons through adequate pseudopotentials in all the following RESP results of the study.

D. Effect of the higher-order terms

In a recent study, Schleife and co-workers [22] produced a high quality ALDA stopping power calculation for aluminum using the time-propagation approach to TDDFT. Their calculations include the perturbation to all orders, whereas ours are limited to the linear response by construction. Hence, the comparison allows us to evaluate the magnitude of the higher-order terms.

In Fig. 8, one can compare our linear-response results to the time-propagation data of Ref. [22] for the traveling of an off-channeled proton in Al, i.e., a proton whose velocity is not aligned with the crystallographic direction of weak density. The differences are indeed rather small, around 5% at most. Considering the conceptual differences in the two approaches and their respective convergence issues, we consider this close match as a confirmation of the linear-response approximation. Surprisingly, the error due to the linear-response approximation does not vary much with the proton velocity. This comparison validates therefore the linear-response approach, at least for protons with velocities larger than 0.5 a.u.

V. RESULTS FOR BULK MATERIALS

With the formalism described above, we can now check the validity of some commonly stated rules of thumb concerning the RESP.

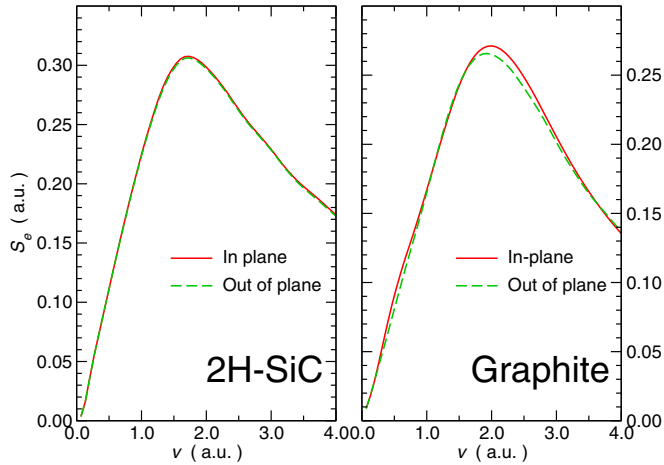


FIG. 9. Anisotropy of the RESP of a proton in 2H-SiC (left-hand panel) and in graphite (right-hand panel) within ALDA including the $2s2p$ electrons of Si.

A. How weak is the RESP anisotropy of anisotropic materials?

With the recent interest in graphene [46], the question about the magnitude of the anisotropy of the RESP is being raised. In an anisotropic material, the RESP depends on the magnitude of the velocity and on its direction. This anisotropy is usually completely disregarded in the interpretation of the experimental data, either because the anisotropy is expected to be small, or because the experimental samples are polycrystalline (and the anisotropy is then averaged out).

We analyze in Fig. 9 the anisotropy of the RESP of two prototypical crystals, 2H-SiC (silicon carbide in wurzite structure) and graphite. Figure 9 shows the RESP along a direction in the plane against the RESP along the out-of-plane axis. The dense structure of wurzite SiC is weakly anisotropic and, as expected, the RESP is almost insensitive to the direction of \mathbf{v} . The layered structure of graphite, which consists in hexagonal planes of carbon separated by a large spacing, may be expected to give rise to a larger anisotropy. However, the RESP in the right-hand panel of Fig. 9 has a very small direction dependence, which amounts to at most 3% in the peak region.

The weak dependence of the RESP can be rationalized by inspecting Eq. (18). In this equation, the imaginary part of ε^{-1} is known to be highly anisotropic for low-energy transfers, as in graphite [47] for instance. However, Eq. (18) is a weighted average of the loss functions for all the values of the transferred momentum $\mathbf{q} + \mathbf{G}$. As seen from Eq. (18), a larger weight $\mathbf{v} \cdot (\mathbf{q} + \mathbf{G})$ is given to those momenta that are parallel to the velocity \mathbf{v} . However, for these transferred momenta, the loss function is evaluated for larger energies $\mathbf{v} \cdot (\mathbf{q} + \mathbf{G})$, at which the anisotropy of the loss function is much weaker.

As a conclusion, the anisotropy of the RESP is always very weak, even for crystal structures which are very anisotropic.

B. Is the Bragg's additivity rule valid?

It has been observed since the early times of particle irradiation [48] that the electronic stopping power is mainly proportional to the average density of electrons, so that

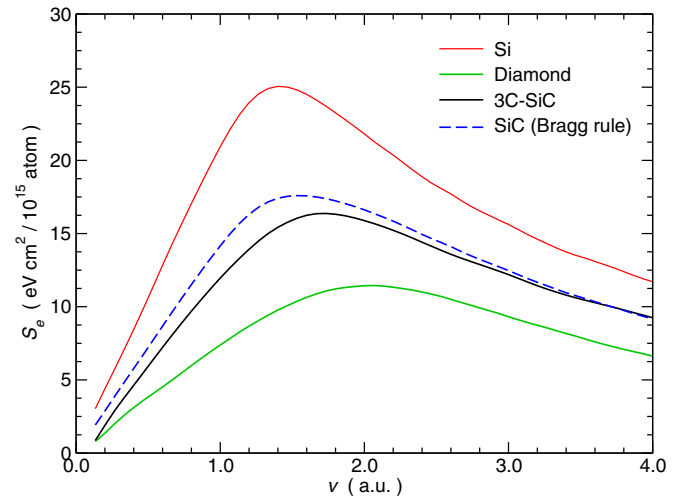


FIG. 10. RESP of a proton in Si, diamond, and 3C-SiC within ALDA including the $2s2p$ electrons of Si. The Bragg's rule SiC (dashed blue line) was obtained using Eq. (23).

the stopping power of compounds could be obtained as a weighted average of the stopping power of its constituents. This statement, known as the Bragg's additivity rule, would read for silicon carbide as

$$\frac{S_e(\text{SiC})}{\rho_{at}(\text{SiC})} = \frac{S_e(\text{Si})}{\rho_{at}(\text{Si})} + \frac{S_e(\text{C})}{\rho_{at}(\text{C})}, \quad (23)$$

where ρ_{at} is the atomic density. From experimental databases, some deviations for this rule are documented [11,49]. However, the deviations mainly occur for light elements, such as the condensed phases of organic polymers.

In Fig. 10, we test the adequacy of Eq. (23) for 3C-SiC (zinc-blende structure). This case should be the simplest case for the Bragg's rule, due to the similarity between the crystals considered here. All three crystals, Si, diamond, and 3C-SiC, have a similar crystal structure (diamond or zinc blende), have the same local environment, and have the same electronic configuration. The Bragg's rule indeed shows its efficacy for the large velocity regime, $v > 2$ a.u. However, for low to moderate velocities, the deviation between the Bragg's rule RESP of SiC and the *ab initio* RESP of SiC is as large as 15%.

This very simple test case sheds light on a significant violation of the Bragg's rule. It casts doubts about the application of this rule of thumb for more complex cases, for instance, when the formal charge varies (oxides), or when the bonding changes (single or double bonds).

C. Is the structural phase effect vanishing?

The empirical Bragg's rule also implies that the details of the crystal structure do not influence much the RESP. We propose to check that assumption for two prototypical examples.

Silicon carbide can crystallize in many different phases, named polytypes. The left-hand panel of Fig. 11 shows the RESP for the 2H-SiC (wurzite) and 3C-SiC (zinc blende). These two phases only differ through the stacking of the planes in the (111) direction. The local environment is exactly the same in the two structures. In order to ease the comparison

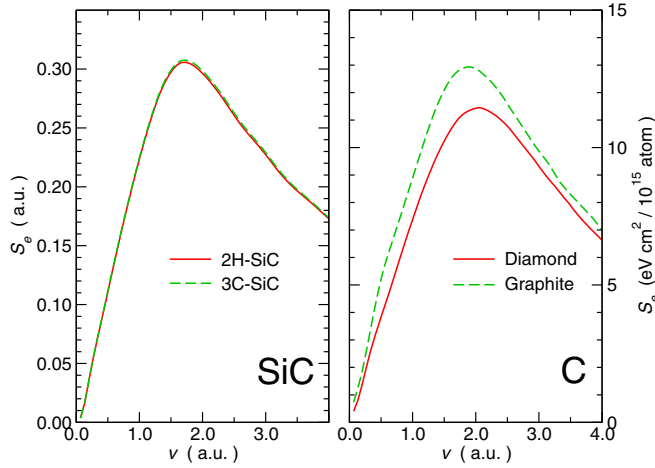


FIG. 11. RESP of a proton in SiC (left-hand panel) and in carbon (right-hand panel) within ALDA including the $2s2p$ electrons of Si. 3C-SiC and 2H-SiC phases are shown for silicon carbide, whereas graphite and diamond phases are shown for carbon. Note that the right-hand panel shows the density renormalized RESP so as to compare two phases with different densities.

between the two, we have used an ideal wurzite structure instead of the experimental structure and we have used a hexagonal supercell of the cubic polytype with six atoms. Finally, the difference in the RESP for the two phases appears to be negligible in the left-hand panel of Fig. 11.

The phases of carbon are a more challenging example. Indeed, the diamond phase of carbon involves tetrahedrally coordinated atoms with sp^3 hybridized electrons, whereas the graphite phase is a layered crystal with sp^2 hybridized electrons. In these two structures, the nature of the bonding is affected and the consequences on the RESP (normalized by the density) are huge as shown in the right-hand panel of Fig. 11. The increase in stopping power of graphite follows the empirical trends highlighted in Ref. [50], which is named the bond effect.

Summarizing, the RESP appears to be sensitive to the details of the bonds, however, the long-range structure is clearly not a relevant parameter, as demonstrated by the different stacking patterns in SiC.

VI. CONCLUSION

In this study, we have developed a numerical approach to calculate the RESP of periodic solids, within the linear-response approach to TDDFT. We have produced high quality stopping power curves with the assistance of an extrapolation technique. We have shown the necessity of a proper description of the core electrons and of the exchange correlation within ALDA. On the basis of a comparison with

the time-propagation results of Ref. [22], we have evaluated an upper limit for the nonlinear effects of 5% in aluminum.

Using the *ab initio* RESP, we have checked some empirical rules of thumb that are commonly employed for the experimental interpretation or for the prediction with empirical codes, such as SRIM [11]. Whereas the anisotropy of the RESP in anisotropic materials can be safely ignored, the Bragg's additivity rule and the phase insensitivity cannot be taken for granted.

ACKNOWLEDGMENTS

This work was performed using HPC resources from GENCI-CCRT-TGCC (Grant No. 2015-096018).

APPENDIX: DERIVATION OF THE LINDHARD FORMULA FROM THE GENERAL CASE OF A PERIODIC CRYSTAL

The homogeneous electron gas is a specific case of a periodic system. It is a periodic system in which all translations are allowed.

Starting from Eq. (18) that involves discrete sums over \mathbf{q} and \mathbf{G} , we go to the limit of a continuous reciprocal space:

$$S_e(\mathbf{v}) = \frac{4\pi Z_1^2}{(2\pi)^3 v} \int d\mathbf{Q} \text{Im}[-\varepsilon^{-1}(Q, \mathbf{Q} \cdot \mathbf{v})] \frac{\mathbf{Q} \cdot \mathbf{v}}{Q^2}, \quad (\text{A1})$$

where $\mathbf{Q} = \mathbf{q} + \mathbf{G}$. Here we have used the fact that the homogeneous electron gas is completely isotropic, i.e., $\varepsilon_{\mathbf{G}\mathbf{G}}^{-1}(\mathbf{q}, \omega) = \varepsilon^{-1}(Q, \omega)$. Equation (A1) precisely corresponds to the equation found in Refs. [51,52].

Let us now introduce spherical coordinates with the z axis along \mathbf{v} . The integration over the azimuthal angle can be readily performed:

$$S_e(\mathbf{v}) = \frac{Z_1^2}{\pi v} \int_0^\infty dQ \int_0^\pi d\theta \sin\theta Q v \cos\theta \times \text{Im}[-\varepsilon^{-1}(Q, Qv \cos\theta)]. \quad (\text{A2})$$

Finally, we apply a change of variable $\omega = Qv \cos\theta$ to obtain the Lindhard formula [9,10]:

$$S_e^{\text{Lindhard}}(\mathbf{v}) = \frac{Z_1^2}{\pi v^2} \int_0^\infty \frac{dQ}{Q} \int_{-Qv}^{Qv} d\omega \omega \text{Im}[-\varepsilon^{-1}(Q, \omega)]. \quad (\text{A3})$$

Sometimes, the parity of integrand is used [since $\varepsilon^{-1}(\omega)$ is causal] to limit the range of integration even further:

$$S_e^{\text{Lindhard}}(\mathbf{v}) = \frac{2Z_1^2}{\pi v^2} \int_0^\infty \frac{dQ}{Q} \int_0^{Qv} d\omega \omega \text{Im}[-\varepsilon^{-1}(Q, \omega)]. \quad (\text{A4})$$

With this derivation we assess that our Eq. (18) is consistent with the derivation of Lindhard and shows that our prefactor which differs from the one in Ref. [16] is correct.

[1] A. A. Correa, J. Kohanoff, E. Artacho, D. Sánchez-Portal, and A. Caro, *Phys. Rev. Lett.* **108**, 213201 (2012).

[2] R. Hatcher, M. Beck, A. Tackett, and S. T. Pantelides, *Phys. Rev. Lett.* **100**, 103201 (2008).

- [3] R. Garcia-Molina, I. Abril, P. de Vera, I. Kyriakou, and D. Emfietzoglou, *J. Phys.: Conf. Ser.* **373**, 012015 (2012).
- [4] P. Sigmund, *Particle Penetration and Radiation Effects—General Aspects and Stopping of Swift Point Charges* (Springer-Verlag, Berlin/Heidelberg, 2006).
- [5] G. S. Was, *Fundamentals of Radiation Materials Science* (Springer-Verlag, Berlin/Heidelberg, 2007).
- [6] M. Born, *Z. Phys.* **38**, 803 (1926).
- [7] H. Bethe, *Ann. Phys. (NY)* **397**, 325 (1930).
- [8] F. Bloch, *Ann. Phys. (NY)* **16**, 285 (1933).
- [9] J. Lindhard, *Mat.-Fys. Medd. K. Dan. Vidensk. Selsk.* **28**, 1 (1954).
- [10] G. J. Iafrate and J. F. Ziegler, *J. Appl. Phys.* **50**, 5579 (1979).
- [11] J. F. Ziegler, J. P. Biersack, and U. Littmark, *The Stopping and Ranges of Ions in Matter* (Pergamon, New York, 1985).
- [12] I. Abril, R. Garcia-Molina, C. D. Denton, F. J. Pérez-Pérez, and N. R. Arista, *Phys. Rev. A* **58**, 357 (1998).
- [13] S. Heredia-Avalos, R. Garcia-Molina, J. M. Fernández-Varea, and I. Abril, *Phys. Rev. A* **72**, 052902 (2005).
- [14] M. D. Barriga-Carrasco, *Phys. Rev. E* **82**, 046403 (2010).
- [15] M. Petersilka, U. J. Gossmann, and E. K. U. Gross, *Phys. Rev. Lett.* **76**, 1212 (1996).
- [16] I. Campillo, J. M. Pitarke, and A. G. Eguiluz, *Phys. Rev. B* **58**, 10307 (1998).
- [17] I. Campillo, J. Pitarke, A. Eguiluz, and A. García, *Nucl. Instrum. Methods Phys. Res., Sect. B* **135**, 103 (1998).
- [18] J. Pitarke and I. Campillo, *Nucl. Instrum. Methods Phys. Res., Sect. B* **164-165**, 147 (2000).
- [19] J. M. Pruneda, D. Sánchez-Portal, A. Arnau, J. I. Juaristi, and E. Artacho, *Phys. Rev. Lett.* **99**, 235501 (2007).
- [20] M. Quijada, A. G. Borisov, I. Nagy, R. Díez Muiño, and P. M. Echenique, *Phys. Rev. A* **75**, 042902 (2007).
- [21] A. Ojanperä, A. V. Krasheninnikov, and M. Puska, *Phys. Rev. B* **89**, 035120 (2014).
- [22] A. Schleife, Y. Kanai, and A. A. Correa, *Phys. Rev. B* **91**, 014306 (2015).
- [23] K. Yabana and G. F. Bertsch, *Phys. Rev. B* **54**, 4484 (1996).
- [24] A. Castro, M. A. L. Marques, and A. Rubio, *J. Chem. Phys.* **121**, 3425 (2004).
- [25] K. Lopata and N. Govind, *J. Chem. Theory Comput.* **7**, 1344 (2011).
- [26] A. Schleife, E. W. Draeger, Y. Kanai, and A. A. Correa, *J. Chem. Phys.* **137**, 22A546 (2012).
- [27] P. M. Echenique, R. M. Nieminen, J. C. Ashley, and R. H. Ritchie, *Phys. Rev. A* **33**, 897 (1986).
- [28] J. C. Ashley, A. Gras-Martí, and P. M. Echenique, *Phys. Rev. A* **34**, 2495 (1986).
- [29] S. L. Adler, *Phys. Rev.* **126**, 413 (1962).
- [30] N. Wisser, *Phys. Rev.* **129**, 62 (1963).
- [31] F. Sottile, F. Bruneval, A. G. Marinopoulos, L. K. Dash, S. Botti, V. Olevano, N. Vast, A. Rubio, and L. Reining, *Int. J. Quantum Chem.* **102**, 684 (2005).
- [32] H.-C. Weissker, J. Serrano, S. Huotari, F. Bruneval, F. Sottile, G. Monaco, M. Krisch, V. Olevano, and L. Reining, *Phys. Rev. Lett.* **97**, 237602 (2006).
- [33] H.-C. Weissker, J. Serrano, S. Huotari, E. Luppi, M. Cazzaniga, F. Bruneval, F. Sottile, G. Monaco, V. Olevano, and L. Reining, *Phys. Rev. B* **81**, 085104 (2010).
- [34] W. M. Saslow and G. F. Reiter, *Phys. Rev. B* **7**, 2995 (1973).
- [35] L. Hedin, *Phys. Rev.* **139**, A796 (1965).
- [36] M. S. Hybertsen and S. G. Louie, *Phys. Rev. B* **34**, 5390 (1986).
- [37] X. Gonze, B. Amadon, P. M. Anglade, J. M. Beuken, F. Bottin, P. Boulanger, F. Bruneval, D. Caliste, R. Caracas, M. Côté, T. Deutsch, L. Genovese, P. Ghosez, M. Giantomassi, S. Goedecker, D. R. Hamann, P. Hermet, F. Jollet, G. Jomard, S. Leroux *et al.*, *Comput. Phys. Commun.* **180**, 2582 (2009).
- [38] J. Paier, M. Marsman, K. Hummer, G. Kresse, I. C. Gerber, and J. G. Ángyán, *J. Chem. Phys.* **124**, 154709 (2006).
- [39] M. Inokuti, *Rev. Mod. Phys.* **43**, 297 (1971).
- [40] E. H. Mortensen, J. Oddershede, and J. R. Sabin, *Nucl. Instrum. Methods Phys. Res., Sect. B* **69**, 24 (1992).
- [41] A. P. Sorini, J. J. Kas, J. J. Rehr, M. P. Prange, and Z. H. Levine, *Phys. Rev. B* **74**, 165111 (2006).
- [42] J. Lindhard and M. Scharff, *Mat.-Fys. Medd. K. Dan. Vidensk. Selsk.* **27**, 1 (1953).
- [43] M. Berger, J. Coursey, M. Zucker, and J. Chang, ESTAR, PSTAR, and ASTAR: Computer Programs for Calculating Stopping-Power and Range Tables for Electrons, Protons, and Helium Ions (version 1.2.3), National Institute of Standards and Technology, Gaithersburg, MD, 2005.
- [44] G. Onida, L. Reining, and A. Rubio, *Rev. Mod. Phys.* **74**, 601 (2002).
- [45] S. Botti, A. Schindlmayr, R. D. Sole, and L. Reining, *Rep. Prog. Phys.* **70**, 357 (2007).
- [46] V. Despoja, K. Dekanić, M. Šunjić, and L. Marušić, *Phys. Rev. B* **86**, 165419 (2012).
- [47] A. G. Marinopoulos, L. Reining, V. Olevano, A. Rubio, T. Pichler, X. Liu, M. Knupfer, and J. Fink, *Phys. Rev. Lett.* **89**, 076402 (2002).
- [48] W. H. Bragg and R. Kleeman, *Philos. Mag. Ser. 6* **10**, 318 (1905).
- [49] D. I. Thwaites, *Radiat. Res.* **95**, 495 (1983).
- [50] J. R. Sabin and J. Oddershede, *Nucl. Instrum. Methods Phys. Res., Sect. B* **27**, 280 (1987).
- [51] T. M. H. E. Tielens, G. E. W. Bauer, and T. H. Stoof, *Phys. Rev. B* **49**, 5741 (1994).
- [52] J. Pruneda, D. Sánchez-Portal, A. Arnau, J. Juaristi, and E. Artacho, *Nucl. Instrum. Methods Phys. Res., Sect. B* **267**, 590 (2009).